Developing an Uncertainty Analysis for Optical Scatterometry

Thomas A. Germer,[a] Heather J. Patrick,[a,b] Richard M. Silver,[a], and Benjamin Bunday[c]

[a]National Institute of Standards and Technology, Gaithersburg, MD 20886 USA
[b]KT Consulting, Antioch, CA 94509 USA
[c]International SEMATECH Manufacturing Initiative (ISMI), Albany, NY 12203 USA

ABSTRACT

This article describes how an uncertainty analysis may be performed on a scatterometry measurement. A method is outlined for propagating uncertainties through a least-squares regression. The method includes the propagation of the measurement noise as well as estimates of systematic effects in the measurement. Since there may be correlations between the various parameters determined by the measurement, a method is described for visualizing the uncertainty in the extracted profile. The analysis is performed for a 120 nm pitch grating, consisting of photoresist lines 120 nm high, 45 nm critical dimension, and 88° side wall angle, measured with a spectroscopic rotating compensator ellipsometer. The results suggest that, while scatterometry is very precise, there are a number of sources of systematic errors that limit its absolute accuracy. Addressing those systematic errors may significantly improve scatterometry measurements in the future.

Keywords: accuracy, optical critical dimension metrology, scatterometry, traceability, uncertainty analysis

1. INTRODUCTION

Optical scatterometry, sometimes referred to as optical critical dimension (OCD) metrology, has become an attractive tool for dimensional metrology in the semiconductor industry, due in large part to its inline potential for providing critical feedback information necessary for tight process control. Until recently, however, little attention has been given to establishing absolute accuracy for optical scatterometry. Instead, most of the effort has focused on the total measurement uncertainty (TMU) methodology,[1,2] whereby accuracy is established by comparison with an independent traceable measurement tool, often atomic force microscopy (AFM).[3,4] Scatterometry, however, performs its measurements in such a different manner than AFM that such comparisons can be misleading. Unlike AFM, which measures the dimensions of a target by physically contacting it, scatterometry measures those dimensions by obtaining an optical signature and comparing that signature to a theoretical model. If a scatterometry measurement disagreed with a traceable standard by some amount, the scatterometer cannot be calibrated by adjusting future values by the difference.

In this paper, we discuss the development of an independent uncertainty budget for optical scatterometry, an important step toward establishing traceability to the International System (SI) meter. Traceability is defined as the "property of a measurement result whereby the result can be related to a reference through a documented unbroken chain of calibrations, each contributing to the measurement uncertainty."[5] In effect, it requires that a traceable measurement have a documented uncertainty budget, for which each term contributing to the uncertainty of the measurement has its own uncertainty budget.

One of the key developments has been a methodology for propagating systematic uncertainties and signal noise through a regression analysis.[6] The regression analysis optimizes a set of floating parameters (e.g., CD, side wall angle, and height) under a set of fixed assumptions (e.g., optical constants and instrument conditions). A scatterometry sensitivity analysis program, OCDSense, has been developed that implements this methodology for any grating structure and measurement scheme. In its current implementation, OCDSense propagates the noise in the reflectance measurement and the uncertainties in the fixed parameters (assumptions) to the covariance matrix of the floating parameters. Uncertainties in incident angle, wavelength, finite target size, roughness, beam focusing, channel cross-talk, and radiometric accuracy also contribute to the measurement uncertainty, and to some extent, these uncertainties can be included in OCDSense as well. A secondary feature

Metrology, Inspection, and Process Control for Microlithography XXIII, edited by John A. Allgair, Christopher J. Raymond
Proc. of SPIE Vol. 7272, 72720T · © 2009 SPIE · CCC code: 0277-786X/09/$18 · doi: 10.1117/12.814835

of an independent uncertainty analysis is that it enables predictions of how scatterometry will behave for new structures. The uncertainty analysis can guide the development of future scatterometers, and it can be used to optimize which parameters are best allowed to float and which are best to fix during library generation or regression analysis. Secondary information, provided by independent measurements or fed forward from previous process steps, can be used to reduce the uncertainties.

2. PROPAGATING UNCERTAINTIES

In this section, we outline the basic methodology used to propagate uncertainties in a scatterometry measurement. This methodology is compatible with the *Guide to the Expression of Uncertainty in Measurement* (GUM),[7,8] but is tailored for use in a regression environment. We will only summarize the results here, providing the details in a separate forthcoming publication.[6]

We assume that the scatterometry signal is being modeled and described with a set of functions $y_i = f_i(\mathbf{a}, \mathbf{b})$ that simulates the value y_i measured for each of N data points. The vector $\mathbf{a} \equiv (a_1, ..., a_M)^{\mathrm{T}}$ represents the M floating measureands estimated by a least-squares regression analysis. The vector $\mathbf{b} \equiv (b_1, ..., b_K)^{\mathrm{T}}$ represents all of the other K fixed values that are input into the model, which should parameterize all significant sources of errors that will propagate to the estimated values $\mathbf{a}$. Often, there are more estimated parameters than are of interest to the user, but it may be recognized that some parameters affecting the outcome are not known sufficiently well to treat them as fixed parameters. In vector form, the function is represented by $\mathbf{y} = \mathbf{f}(\mathbf{a}, \mathbf{b}) \equiv [f_1(\mathbf{a}, \mathbf{b}), ..., f_N(\mathbf{a}, \mathbf{b})]^{\mathrm{T}}$.

The fixed parameters $\mathbf{b}$, while being fixed during the regression analysis, all have estimated variances and covariances associated with them, which we will assume are expressed in matrix form as

$$\mathbf{u}^2(\mathbf{b}) = \langle \mathbf{b}\mathbf{b}^{\mathrm{T}} \rangle - \langle \mathbf{b} \rangle \langle \mathbf{b}^{\mathrm{T}} \rangle. \tag{1}$$

Furthermore, each of the measurements $\mathbf{y}$ have variances and covariances given in matrix form as $\mathbf{u}^2(\mathbf{y})$, in a similar manner as $\mathbf{u}(\mathbf{b})$ above. The matrices $\mathbf{u}^2(\mathbf{b})$ and $\mathbf{u}^2(\mathbf{y})$ are often treated as diagonal, but they do not have to be. Our task is to determine how these estimated variances and covariances propagate into an estimated variance-covariance matrix $\mathbf{u}^2(\mathbf{a})$ of the estimated parameters, $\mathbf{a}$.

A weighted least-squares regression analysis compares the data to the theoretical model and estimates the parameters $\mathbf{a}$ by minimizing the value[9,10]

$$\chi^2 = \sum_i w_i [y_i - f_i(\mathbf{a}, \mathbf{b})]^2, \tag{2}$$

where the w_i are weighting factors. Usually, if the variances $u^2(y_i)$ are known, the weighting factors are chosen to be $w_i = 1/u^2(y_i)$, but this does not necessarily have to be the case. We can write Eq. (2) as a matrix expression

$$\chi^2 = [\mathbf{y} - \mathbf{f}(\mathbf{a}, \mathbf{b})]^{\mathrm{T}} \mathbf{W} [\mathbf{y} - \mathbf{f}(\mathbf{a}, \mathbf{b})], \tag{3}$$

where $\mathbf{W}$ is an $N \times N$ diagonal matrix with diagonal elements w_i. If $\mathbf{a} = \mathbf{a}_{\min}$ minimizes χ^2, then we consider $\mathbf{a}_{\min}$ to be an estimate of the true value of $\mathbf{a}$. We will not discuss the various methods that are used to perform this minimization, because all we need to know is that such a minimum exists and that the functions $f_i(\mathbf{a}, \mathbf{b})$ are sufficiently smooth that they can be Taylor series expanded about that minimum. If we assume that all of the errors are normally distributed, that the functions $f_i(\mathbf{a}, \mathbf{b})$ are sufficiently well represented by their first, linear terms in their expansion, that the errors in the measurements of $\mathbf{y}$ have zero mean (that is, any systematic errors are incorporated in a term in $\mathbf{b}$), that the weighting function is chosen to be the inverse of the variance of each of the measurements, and that the measurements are uncorrelated, then we can show that the covariance matrix of $\mathbf{a}$ resulting from the covariance matrix $\mathbf{u}^2(\mathbf{y})$ is

$$\mathbf{u}_{\mathrm{a}}^2(\mathbf{a}) = (\mathbf{A}^{\mathrm{T}} \mathbf{A})^{-1}. \tag{4}$$

where the elements of the matrix $\mathbf{A}$ are

$$A_{ij} = w_i^{1/2} \frac{\partial f_i(\mathbf{a}', \mathbf{b}')}{\partial a_j'} \bigg|_{\mathbf{a}'=\mathbf{a}_{\min}, \mathbf{b}'=\mathbf{b}}, \tag{5}$$

When we consider errors in $\mathbf{b}$, which we will take to be systematic errors, at least from the perspective of the least-squares regression, we find

$$\delta\mathbf{a} = -\mathbf{A}^{+}\mathbf{B}\delta\mathbf{b}, \tag{6}$$

where the elements of the matrix $\mathbf{B}$ are

$$B_{ik} = w_i^{1/2} \frac{\partial f_i(\mathbf{a}', \mathbf{b}')}{\partial b_k'}\bigg|_{\mathbf{a}'=\mathbf{a}_{\min},\mathbf{b}'=\mathbf{b}} \tag{7}$$

and

$$\mathbf{A}^{+} = (\mathbf{A}^{\mathrm{T}}\mathbf{A})^{-1}\mathbf{A}^{\mathrm{T}}. \tag{8}$$

($\mathbf{A}^{+}$ is often referred to as the left-pseudoinverse of $\mathbf{A}$.) The variance-covariance matrix resulting from the systematic errors in the system is given by

$$\mathbf{u}_{\mathrm{b}}^2(\mathbf{a}) = \langle \delta\mathbf{a}\delta\mathbf{a}^{\mathrm{T}} \rangle = \mathbf{A}^{+}\tilde{\mathbf{B}}\mathbf{u}^2(\mathbf{b})\mathbf{B}^{\mathrm{T}}(\mathbf{A}^{+})^{\mathrm{T}}, \tag{9}$$

where $\mathbf{u}^2(\mathbf{b}) = \langle \delta\mathbf{b}\delta\mathbf{b}^{\mathrm{T}} \rangle$ is the variance-covariance matrix of the parameters $\mathbf{b}$.

The combined uncertainty in the measurement is obtained using the guidance of the GUM by combining the variance-covariance matrices obtained above,[7,8]

$$\mathbf{u}_{\mathrm{c}}^2(\mathbf{a}) = \mathbf{u}_{\mathrm{a}}^2(\mathbf{a}) + \mathbf{u}_{\mathrm{b}}^2(\mathbf{a}). \tag{10}$$

Finally, the expanded uncertainty in the ith estimated parameter is

$$U(a_i) = k\sqrt{[\mathbf{u}_{\mathrm{c}}^2(\mathbf{a})]_{ii}} \tag{11}$$

where k is a coverage factor, often chosen to be 2 or 3, depending upon the level of confidence desired.

In scatterometry, we are often interested in knowing what structures lie within the measurement and the uncertainty. In many cases, it is difficult to appreciate the uncertainties in a particular parameter, without knowing how the other parameters are allowed to vary. Here, it is useful to consider a combined covariance matrix, given by

$$\mathbf{u}^2[(\mathbf{a},\mathbf{b})^{\mathrm{T}}] = \begin{pmatrix} \mathbf{u}_{\mathrm{c}}^2(\mathbf{a}) & -\mathbf{A}^{+}\mathbf{B}\mathbf{u}^2(\mathbf{b}) \\ -\mathbf{u}^2(\mathbf{b})(\mathbf{A}^{+}\mathbf{B})^{\mathrm{T}} & \mathbf{u}^2(\mathbf{b}) \end{pmatrix}. \tag{12}$$

We can generate multivariate random numbers that reproduce the statistics described by Eq. (12). Such a random number generator can be realized by finding the eigenvectors and the eigenvalues of the covariance matrix, creating normally-distributed random numbers having variances given by the eigenvalues, and multiplying those random numbers by the corresponding eigenvectors. Armed with the ability to generate random profiles that are measurably equivalent, we now have a powerful visualization technique in our analysis arsenal.

We developed a computer program, OCDSense, to perform the analysis described above. It takes a parameterized grating structure along with descriptions of the measurement, estimates of the noise in the measurement, and estimates for the independent uncertainties in each of the parameters and returns the uncertainty budget for those parameters chosen to be estimated. It also can provide the estimated covariance matrix and realizations of the profile as described above. Finally, besides just the profile description, it also allows propagation of a number of systematic errors, such as those due to the angle of incidence, the rotation of the grating, and the wavelength scale. OCDSense uses rigorous coupled wave (RCW) analysis to perform the electromagnetic simulations.[11–14]

The various uncertainties input into OCDSense are expected to represent the estimated standard deviations of the respective parameters. Often, instead of having that information, we have fixed ranges $[b_i - \Delta, b_i + \Delta]$, over which we can expect a parameter b_i to vary. Following the GUM, we assume that the distribution is uniform over that range, and that the estimated standard deviation is given by 0.58Δ.

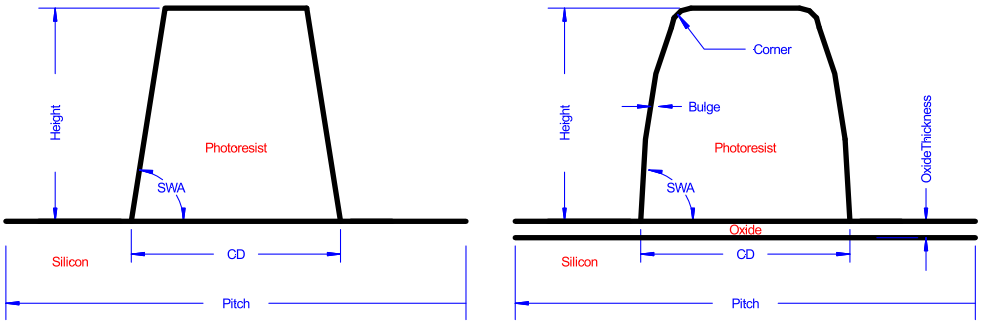

Figure 1. Two profiles describing a photoresist line above a silicon substrate. On the left is a simplified model that would be used to fit experimental data. On the right is a more complex model, assumed to be a more realistic model, used for analyzing the uncertainties.

3. EXAMPLE PROFILE AND TOOL

In this article, we will use a virtual sample and virtual tool to illustrate how a specific uncertainty analysis would proceed. In the future, however, the methods described here will be applied to real samples and tools, using component uncertainties determined appropriately. Thus, the specific values used here are only an estimate of what might be expected in a realistic measurement.

The target grating profile that we will use is a trapezoidal photoresist line on top of a silicon substrate. The photoresist has a nominal bottom width (CD) of 45 nm, a side wall angle (SWA) of 88° and a height of 120 nm. The pitch of the grating is 120 nm. A single period of the grating is illustrated in Fig. 1.

The scatterometry tool will be a rotating compensator spectroscopic ellipsometer operating from 200 nm to 900 nm with the light dispersed in steps of 2 nm. The incident angle is 70°, and the grating vector is in the plane of incidence (the so-called normal diffraction geometry). As a rotating compensator ellipsometer, the signal consists of four components: a dc component, one at twice the rotation frequency ($2f$) of the compensator (a sine component), and two at four times the rotation frequency ($4f$) of the compensator (sine and cosine). The least-squares minimization analysis is considered on the ratio of each of the three ac signals to the dc signal.

4. SOURCES OF UNCERTAINTY

There are a number of sources of uncertainty in scatterometry measurements. In this section, we will enumerate a number of them, and discuss how they affect the uncertainty in the final measurement.

4.1 Signal noise

The reproducibility of the measurement is encapsulated by the covariance matrix $\mathbf{u}_{\mathrm{a}}^2(\mathbf{a})$ given in Eq. (4) above. The behavior of $\mathbf{u}_{\mathrm{a}}^2(\mathbf{a})$ is by far the most studied term in the total covariance matrix.[15] It is relatively simple to calculate, given either the measured noise statistics or by simply performing a measurement on a tool multiple times and viewing the resulting distribution of extracted profiles.

Precision is one of the key attractions of scatterometry for process control monitoring. Generally, the lower the number of floating parameters, the higher the tool precision. As more parameters are added to those floating, the precision degrades. On the other hand, if the floating parameters do not cover the range of realistic process variations, then the accuracy may be substantially lower than that estimated by Eq. (4).

For this study, we obtained a characteristic noise spectrum for a tool and smoothed it by hand. The resulting noise, shown in Fig. 2 as a function of wavelength, was applied to each of the four measured signals. Since each derived measurement y_i is the ratio of two measured signals (i.e., $y_i = r_i/s_i$), we calculate the uncertainty in y_i according to standard procedures to be

$$u(y_i) = \frac{\sqrt{r_i^2 u^2(r_i) + s_i^2 u^2(s_i)}}{s_i^2}, \tag{13}$$

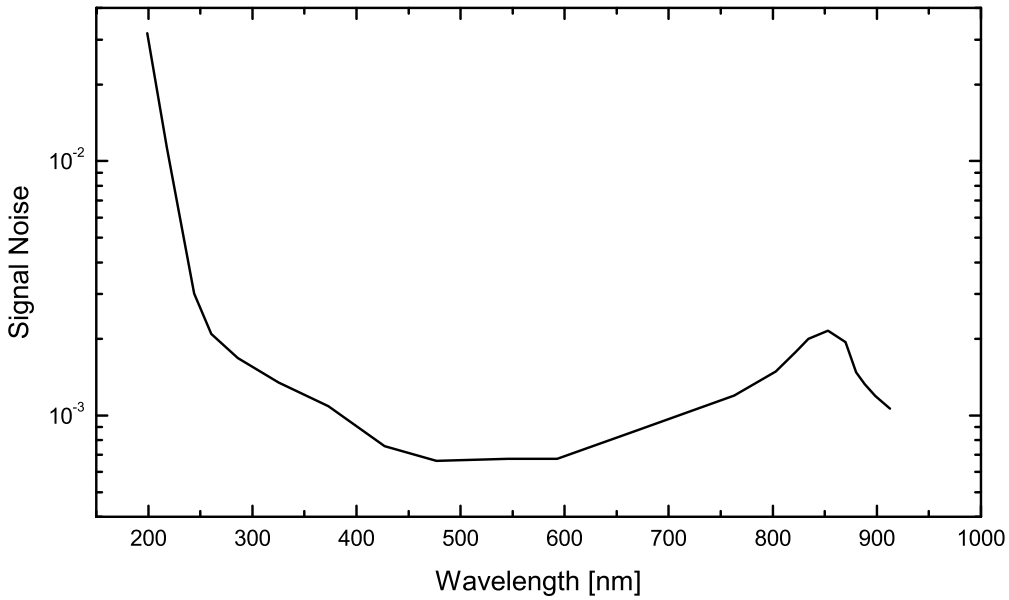

Figure 2. The noise spectrum, expressed as the standard deviation of each of the four component measurements (dc and ac components), assumed for the uncertainty analysis.

where $u^2(r_i)$ and $u^2(s_i)$ are the variances of r_i and s_i, respectively, which here we assume to be the same. This noise level was also assumed to be used to determine the weighting function during the least-squares analysis. This spectrum has a couple characteristic features, namely the noise has a peak in the near infrared, where the detector responsivity is low and the thermal part of the lamp output is low, and diverges in the ultraviolet, where the detector responsivity and the lamp output both drop.

4.2 Profile Parameterization

One of the largest uncertainties associated with the scatterometry measurement is that associated with the profile parameterization. The structure is constrained by the profile model, which may not reflect the true structure.

Consider our simple structure, shown on the left in Fig. 1, consisting of a photoresist line grating on top of a silicon substrate. For the analysis of the data, the user may choose to parameterize the structure in terms of a critical dimension (CD), a side wall angle (SWA), and a height. While the user is increasing the precision in the measurement by keeping the number of parameters small, there are many assumptions that the user is making that will have an effect on the total accuracy. For example, the pitch, while probably fixed in the production process, is not known to infinite accuracy and may even vary to a small extent with exposure focus. The side wall may not be straight, but rather may be bulged or indented to some degree. The corners of the structures may have some rounding, if only because of surface tension. The substrate is likely to have a native oxide on it. On the right in Fig. 1, we show an alternative profile description, which would be appropriate for analysis by OCDSense. Each of the additional parameters represents systematic variables that need to have uncertainties assigned to them. Such information would be provided by off-line metrologies, such as AFM or cross sectional scanning electron microscopy (SEM), together with experience from process engineers.

For the pitch, we assumed that it was within 1 nm of its nominal value, so that its estimated standard deviation was 0.3 nm. For the amount of bulge, we assumed that a 1 nm standard deviation would be a reasonable level. The vertices of the bulge are fixed at one-third and two-thirds of the height (allowing these to vary, too, would require that we consider correlations between the bulge distance and these heights). The corner rounding radius was assumed to be in the range $[0\text{ nm}, 4\text{ nm}]$; thus, the center value was assumed to be 2 nm, with an estimated standard uncertainty 1.2 nm. The oxide thickness was assumed to be in the range $[1\text{ nm}, 2\text{ nm}]$; thus, the center value was assumed to be 1.5 nm, with an estimated standard uncertainty 0.3 nm.

4.3 Optical properties

The line profile description also contains information about the optical properties of the materials in the grating. In our example grating, one should propagate the uncertainties arising from errors in the optical properties of the photoresist, the oxide layer, and the substrate. In the case of the silicon substrate, we can find two literature curves for the silicon optical properties, $\tilde{n}_{\mathrm{Si1}}(\lambda)$ and $\tilde{n}_{\mathrm{Si2}}(\lambda)$, and assume that the real optical constants vary between them.[16,17] Thus, we assume that

$$\tilde{n}_{\mathrm{Si}}(x,\lambda) = x\tilde{n}_{\mathrm{Si1}}(\lambda) + (1-x)\tilde{n}_{\mathrm{Si2}}(\lambda) \tag{14}$$

where x is a parameter in the range $[0,1]$. Thus we assume $\langle x \rangle = 0.5$ and $u(x) = 0.3$. The index of refraction of the oxide layer may vary in a similar way between values for bulk silicon dioxide and those reported in the literature for a native silicon oxide.[16,17] In the case of the photoresist, we could do a similar expansion of the optical properties. However, we do not have sufficient information about the range of indices. Since the photoresist is primarily a dielectric, we might assume instead that the index is given by

$$\tilde{n}(x,\lambda) = (1+x)\tilde{n}_1(\lambda) \tag{15}$$

where x is now a small number assumed to vary about zero. We let $\langle x \rangle = 0$ and $u(x) = 0.005$ for the photoresist.

In some cases, especially where process variations exist in the materials, the parameters controlling the optical properties could be treated as floating parameters in the scatterometry measurement. While the optical properties are dependent upon wavelength, the process variation of many materials has a low dimensionality. For example, the complex index of refraction of poly-silicon[18] can be treated as a continuous set of curves parameterized by the volume fraction of amorphous silicon. Thus, the addition of process variation may not require the addition of many new floating parameters, and yet the accuracy gained by including them may be substantial.

4.4 Measurement uncertainties

There are several measurement uncertainties that can occur. These are generally ignored by the user and left to the tool vendor to characterize, and usually fall under the category of tool or fleet matching. In this section, we discuss the most likely sources of error in the measurement and make estimates of their uncertainties.

4.4.1 Wavelength

Ultimately, scatterometry transfers the wavelength scale used for the measurement to the dimensional parameters associated with the target structure. All other effects being constant (most notably the optical properties of the materials), a uniform error in the wavelength of 1 % should result in a 1 % error in all of the dimensions of the structure. These errors, however, can become magnified because many of the materials have optical properties that impart structure onto the optical signature. If there is an error in the apparent wavelengths of those spectral features, other parameters attempt to compensate.

For laser-based, fixed wavelength tools, the uncertainty from the wavelength may contribute insignificantly to the final result. Gas lasers, for example, often have wavelength uncertainties, even without stabilization, of better than 0.001 nm. However, spectral instruments generally rely upon a calibrated spectrometer and cannot be expected to perform much better than about 0.25 times their spectral resolution. We thus assume, for our virtual spectrometer, that the estimated standard deviation of the wavelength is given by 0.3 nm, and that it is modeled with a uniform shift.

4.4.2 Angle of incidence

The scatterometry signature depends upon the angle of incidence. Because the light source must be focused relatively tightly onto the sample, there is a conical spread in those incident angles, and the theoretical analysis may or may not take this into account. In either case, the central angle of incidence can be determined by using a film standard with known optical properties and thickness. Using this method will determine the intensity- and reflectance-weighted angle of incidence for the instrument, which may differ from the intensity- and reflectance-weighted angle of incidence for the grating. For our simulations, we let the maximum error in the angle of incidence be 0.05°, corresponding to an estimated standard deviation of 0.03°.

4.4.3 Sample rotation

Like angle of incidence, the scatterometry signature depends upon the rotation angle of the sample. However, that angle cannot be found using a film standard. Some rotating compensator spectroscopic ellipsometers perform zone-averaging, so that the incident polarization is switched between 45° and −45°, with the results averaged. In this case, the resulting error from the sample rotation is insignificant, the result having a quadratic effect on angle rather than a linear effect. For this study, however, we will assume that the maximum error from the sample rotation is about 0.1°, corresponding to an estimated standard deviation of 0.06°.

4.4.4 Photometric accuracy

In this section, we refer to issues associated with the measureands directly. If we are measuring the ratio of ac signals to dc signals, we need to consider whether those signals are appropriately calibrated with respect to one another. For this study, we will assume that these ratios are accurate to 0.1 %, similar to the noise level, corresponding to an estimated standard deviation of 0.06 %. Since the ac signals are phase-sensitive, we also include the possibility that the phases have an uncertainty. The phase for the $2f$ signal is effectively included in the ratio uncertainty , while we include a $[-0.5°, 0.5°]$ range in the phase of each of the $4f$ signals.

4.5 Electromagnetic simulation accuracy

Scatterometry measurements rely upon the electromagnetic modeling being accurate. RCW simulations, however, make a number of approximations. One of those approximations is the so-called staircase approximation, whereby sloping interfaces are approximated by a finite number of layers, each having vertical interfaces. There is some question about the validity of this approximation in the literature, although most of the problems have been associated with very shallow interfaces, like one would have in a blazed grating, and for metallic materials.[19] RCW also approximates the electric and magnetic fields in each layer by expanding each of them in a Floquet series, which must be truncated to perform the simulation on a computer. While some problems existed in the past, associated with transverse magnetic (TM) waves incident on the grating,[12,13] convergence can still be relatively slow, especially for metallic gratings. A number of comparisons have been made between different scattering methodologies, including RCW, finite difference, finite element, and another modal method, and generally good results were obtained.[20]

To estimate the effects of simulation accuracy on the measurement, we do the simulation, truncating the Floquet series at ±10 orders, and compare the results with those obtained with ±20 orders. Furthermore, we compare the results dividing the structure into 10 layers and compare the results with 15 layers. For the photoresist structure used here, convergence is fairly quick and the larger values can be safely assumed to represent truth, while the smaller values would be required to make the computation time of a measurement reasonable.

4.6 Other considerations

In this subsection, we will discuss a number of issues that are much more difficult to assess, but which need to be considered for a serious uncertainty budget. These are issues that require significantly more computation power and assumptions to evaluate. Furthermore, these errors can depend upon the sample being measured, and thus do not fall under the realm of tool matching. We will not include any of these uncertainties in our budget, but we will list them.

4.6.1 Finite target size

The targets used in many scatterometry measurements are very small, usually less than 100 μm on a side and often less than 50 μm on a side. At these dimensions, some light is bound to spill over beyond the target and illuminate the region surrounding the target, if not other adjacent structures. Kenyon, *et al.*, considered such effects by treating the signal as a sum of the diffraction by the target and the diffraction by the surrounding region.[21] The results suggested that incoherent collection of the reflected light with little or no occlusion minimized the effects from the outside region. However, any occlusion of the beam necessarily increased the coherent addition of the signal arising from the surrounding region with that from the target and can cause shifts in the results.

Table 1. Uncertainty budget determined using the arguments outlined in this article.

	CD [nm]	SWA [deg]	Height [nm]
Type A Uncertainties			
Instrument noise	0.04	0.02	0.03
Type B Uncertainties			
Pitch	−0.75	0.37	−0.68
Bulge	1.02	0.28	−0.82
Corner radius	−0.02	0.01	−0.08
Photoresist, optical properties	0.19	0.33	−0.63
Oxide, optical properties	−0.42	0.20	−0.22
Oxide, thickness	0.42	−0.18	0.47
Silicon optical properties	−0.15	0.07	−0.13
Model, maximum field order	−0.00	0.00	−0.00
Model, number of layers	0.03	−0.01	−0.00
Wavelength scale	0.29	−0.17	0.20
Sample rotation	−0.03	0.01	−0.01
Incident angle	0.18	−0.02	−0.20
Tool, $\sin(2f)$ scale	0.06	−0.03	0.06
Tool, $\cos(4f)$ scale	−0.02	0.01	−0.01
Tool, $\sin(4f)$ scale	−0.02	0.01	0.01
Tool, $\cos(4f)$ phase	0.29	−0.11	0.09
Tool, $\sin(4f)$ phase	−0.13	0.05	−0.01
Total Type B	1.49	0.67	1.38
Combined	1.49	0.67	1.38
Expanded ($k = 2$)	2.98	1.34	2.76

4.6.2 Line width/Line edge roughness

The effects of line width and line edge roughness have not been studied in great detail. However, it is one of the primary reasons why AFM and scatterometry measurements are very difficult to compare. AFM measures the line profile through a small number of cross sections, while scatterometry measures a weighted average over a much larger area. Work by Germer has investigated line edge and line width roughness in the long period regime and found that the results can be approximated by a incoherent average of line widths.[22,23] More recent results by Bergner, et al., investigated roughness in the short period regime and found that the results could be modeled with an effective medium layer, provided the layer was treated as a birefringent effective medium.[24]

4.6.3 Stray light in spectrometer

Spectrometer-based systems have the potential for exhibiting cross talk between the wavelength channels. For example, accurate colorimetry measurements are very difficult to perform with single-slit, multidetector spectrometers.[25] Little attention has been given to this effect in ellipsometry measurements, no less scatterometry measurements. To estimate these effects, one can assume a point spread function on the detector that illuminates not just the detector in question, but also adjacent and far reaching detectors.

5. RESULTS

We consider the grating shown above in Fig. 1 measured by the spectroscopic rotating compensator ellipsometer described above. We performed the uncertainty analysis, using the component uncertainties and measurement

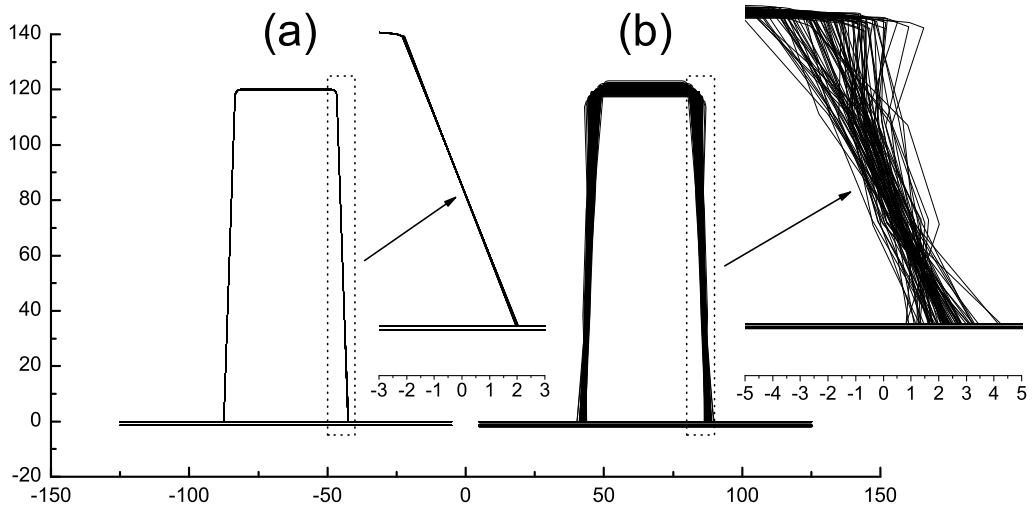

Figure 3. Realizations of the profile consistent with the covariance matrices determined by propagating the uncertainties. The profiles in (a) are those determined solely by propagating the measurement noise through the analysis and represent the Type A uncertainties. The profiles in (b) are those determined by propagating all of the uncertainties listed in Table I. The insets show the details of the side wall profile using an expanded horizontal scale. All of the values are expressed in nanometers.

noises given in Sec. 4. The resulting uncertainties are shown in Table 1. The results are divided into the Type A and Type B components, as defined in the GUM.[7,8]

The results given in Table 1 show that the precision of the measurement, as judged by the Type A uncertainty, can be significantly sub-nanometer. What is striking from the table is how the various possible sources of systematic error contribute to an overall accuracy that is much larger. The expanded uncertainty (coverage factor $k = 2$) is about 6 % of the CD. That uncertainty is dominated by the bulge parameter, that is, the uncertainty in knowing that the side wall is flat. Shortly behind that are the uncertainties in pitch, wavelength, and the properties of the native oxide.

The problem with the uncertainty budget as presented in Table 1 is that it does not represent the correlation between the different parameters. When there are more than a couple floating parameters, it is difficult to appreciate these correlations by looking at the covariance matrix with unaided eye, that is, without performing a principal component analysis. On the other hand, as described above, we can generate multivariate random numbers that replicate the statistics found in the covariance matrix. By doing that and plotting a large number of instances of profiles, we can view how the different parameters are coupled. Figure 3 shows results of such an analysis. On the left of Fig. 3 is shown the distribution of profiles calculated using only the Type A contributions to the covariance matrix, $\mathbf{u}_{\mathrm{a}}^2(\mathbf{a})$. The results show how all three parameters, the CD, SWA, and height are all correlated, essentially ensuring that the total volume of the profile is preserved. On the right side of Fig. 3 is show the distribution of profiles calculated using the full combined covariance matrix, given in Eq. 12.

One can improve the combined uncertainty in CD, SWA, or height by allowing other parameters to be varied in the fit as well. OCDSense allows the user to specify any number of parameters to be "optimized." These parameters are turned on and off, in order to minimize a specified figure of merit. In effect, this procedure allows one to decide whether to leave any given variable fixed, but with a given uncertainty, or letting it float. If the uncertainty in a parameter can be reduced by letting it float, it is better to float that parameter. However, adding parameters to the list of those floating increases the Type A uncertainties, while decreasing the Type B uncertainties. By optimizing the choice of floating parameters, we can, in effect, balance the Type A and Type B uncertainties. If we let all of the grating-definition variables (pitch, bulge, corner radius, oxide thickness and optical properties, photoresist optical properties, and silicon optical properties) be optimized in this way, then

we find that we can reduce the standard combined uncertainty in CD from 1.5 nm to 0.9 nm. The Type A standard uncertainty, however, rises from 0.04 nm to about 0.3 nm.

6. CONCLUSIONS

We have developed a systematic method for establishing the uncertainty in a scatterometry measurement. By considering a number of possible sources of uncertainty, we can identify which sources would contribute greatest to limiting the accuracy of the technique. Furthermore, this study represents an important step needed to produce reference materials for scatterometry and to provide traceability to the SI.

REFERENCES

[1] Banke, Jr., G.W. and Archie, C.N., "Characteristics of accuracy for CD metrology," in *Metrology, Inspection, and Process Control for Microlithography XIII*, B. Singh, ed., Proc. SPIE **3677**, 291–308 (1999).

[2] Bunday, B., Azordegan, A., Banke, B., Archie, C., Solecky, E., Kim, K.-W., Allgair, J., and Silver, R., "Unified Advanced Optical Critical Dimension (OCD) Scatterometry Specification for sub-65 nm Technology (2008 version)." Non-confidential document available at www.sematech.org. ISMI TTID: 04114596F-ENG, Jan 2009.

[3] Sendelbach, M., Archie, C.N., Banke, B., Mayer, J., Nii, H., Herrera, P., and Hankinson, M., "Correlating scatterometry to CD-SEM and electrical gate measurements at the 90-nm node using TMU analysis," in *Metrology, Inspection, and Process Control for Microlithography XVIII*, Richard M. Silver, ed., Proc. SPIE **5375**, 550–563 (2004).

[4] Ukraintsev, V.A., "A comprehensive test of optical scatterometry readiness for 65 nm technology production," in *Metrology, Inspection, and Process Control for Microlithography XX*, C.N. Archie, ed., Proc. SPIE **6152**, 61521G (2006).

[5] *International vocabulary of metrology – Basic and general concepts and associated terms (VIM)*, ISO/IEC Guide 99:2007 (ISO, Geneva, 2007).

[6] Germer, T.A., to be published.

[7] *ISO Guide to the Expression of Uncertainty in Measurement*, (ISO, Geneva, 2006).

[8] Taylor, B.N., and Kuyatt, C.E., "Guidelines for Evaluating and Expressing the Uncertainty of NIST Measurement Results," NIST Technical Note 1297(1994).

[9] Bevington, P.R., and Robinson, D.K., *Data Reduction and Error Analysis for the Physical Sciences*, Second Edition, (McGraw-Hill, New York, 1992).

[10] Press, W.H., Teukolsky, S.A., Vetterling, W.T., and Flannery, B.P., *Numerical Recipes in C*, Second Edition, (Cambridge Univerisity Press, Cambridge, 1992).

[11] Moharam, M.G., Pommet, D.A., Grann, E.B., and Gaylord, T.K., "Stable implementation of the rigorous coupled-wave analysis for surface-relief gratings: enhanced transmittance matrix approach," J. Opt. Soc. Am. A **12**, 1077–1086 (1995).

[12] Lalanne, P., and Morris, G.M., "Highly improved convergence of the couple-wave method for TM polarization," J. Opt. Soc. Am. A **13**, 779–784 (1996).

[13] Li, L., "Use of Fourier series in the analysis of discontinuous periodic structures," J. Opt. Soc. Am. A **13**, 1870–1876 (1996).

[14] Germer, T.A., SCATMECH: Polarized Light Scattering C++ Class Library, version 6, available from `http://physics.nist.gov/scatmech`.

[15] Al-Assaad, R.M., and Byrne, D.M., "Error analysis in inverse scatterometry. I. Modeling," J. Opt. Soc. Am. A **24**, 326–338 (2007).

[16] Herzinger, C.M., Johs, B., McGahan, W.A., Woollam, J.A., and Paulson, W., "Ellipsometric determination of optical constants for silicon and thermally grown silicon dioxide via a multi-sample, multi-wavelength, multi-angle investigation," J. Appl. Phys. **83** , 3323–3336 (1998).

[17] Palik, E.D., *Handbook of Optical Constants of Solids*, (Academic, San Diego, 1985).

[18] Jellison, G.E., Chisholm, M.F., Gorbatkin, S.M., "Optical functions of chemical-vapor-deposited thin-film silicon determined by spectroscopic ellipsometry," Appl. Phys. Lett. **62**, 3348–3350 (1993).

[19] Popov, E., Nevière, M., Gralak, B., and Tayeb, G., "Staircase approximation validity for arbitrary-shaped gratings," J. Opt. Soc. Am. A **19**, 33–42 (2002).

[20] Silver, R., Germer, T., Attota, R., Barnes, B.M., Bunday, B., Allgair, J., Marx, E., and Jun, J., "Fundamental limits of optical critical dimension metrology: A simulation study," in *Metrology, Inspection, and Process Control for Microlithography XXI*, C.N. Archie, ed., Proc. SPIE **6518**, 65180U (2007).

[21] Kenyon, E., Cresswell, M.W., Patrick, H.J., and Germer, T.A., "Modeling the effect of finite size gratings on scatterometry measurements," in *Metrology, Inspection, and Process Control for Microlithography XXII*, Proc. SPIE **6922**, 69223P (2008).

[22] Germer, T.A., "Effect of line and trench profile variation on specular and diffuse reflectance from a periodic structure," J. Opt. Soc. Am. A **24**, 696–701 (2007).

[23] Germer, T.A., "Modeling the effect of line profile variation on optical critical dimension metrology," in *Metrology, Inspection, and Process Control for Microlithography XXI*, Proc. SPIE **6518**, 65180Z (2007).

[24] Bergner, B.C., Suleski, T.J., and Germer, T.A., "Effect of line width roughness on optical scatterometry measurements," Proc. SPIE **7272**, to be published (2009).

[25] Early E.A., and Nadal, M.E., "Uncertainty Analysis of Reflectance Colorimetry," Color Res. Appl. **29**, 205–216 (2004); Early, E.A., and Nadal, M.E., "Uncertainty Analysis for the NIST 0:45 Reflectometer," Color Res. Appl. **33**, 100–107 (2008).